Topological defects in schlieren textures of biaxial and uniaxial nematics

C. Chiccoli,[1] I. Feruli,[2] O. D. Lavrentovich,[3] P. Pasini,[1] S. V. Shiyanovskii,[3] and C. Zannoni[2]

[1]*Istituto Nazionale di Fisica Nucleare, Sezione di Bologna, Via Irnerio 46, 40126 Bologna, Italy*
[2]*Dipartimento di Chimica Fisica and INSTM, Università di Bologna, Viale Risorgimento 4, 40136 Bologna, Italy*
[3]*Liquid Crystal Institute and Chemical Physics Interdisciplinary Program, Kent State University, Kent, Ohio 44242*

Monte Carlo and theoretical studies of thin 3D films of biaxial and uniaxial nematics with tangential boundary conditions show distinct differences in structure and evolution of topological defects. In the uniaxial films, defects of strength $k = \pm 1$ are point defects that bear no bulk singularity and disappear by annihilation with each other. In the biaxial films, $k = \pm 1$ defects are true singular bulk disclinations that split into pairs of $k = \pm 1/2$ lines; the latter disappear by annihilation processes of the type $+1/2-1/2=0$. These observed differences are of relevance for the current debate on the existence of biaxial phases.

Biaxial nematics (BNs) are currently the target of a fascinating and controversial search [1]. They have been predicted by theory [2] and observed by computer simulations for lattice [3], hard core [4], and attractive-repulsive Gay-Berne [5] systems, but their existence in real thermotropics is still questioned [6]. In particular, deuterium NMR (DNMR) could not find evidence of phase biaxiality [7,8] in various mesogens claimed to be BN on the basis of conoscopy. While the interpretation of DNMR is straightforward, the method is not very sensitive to small biaxialities and thus a complementary reliable and sensitive optical technique would be highly desirable to establish the existence or not of this new phase of matter. Optical probing of topological defects is of special interest, since the symmetry difference of biaxial and uniaxial order might lead to drastic differences in the properties of defects in BN and uniaxial nematics (UNs) [9,10]. Chandrasekhar *et al.* [11], noticed that polarizing-microscope textures of their candidate BN contained only defects of half integer and never of integer strength. Since the UN phase shows defects of both types, the observation was suggested as a diagnostic test for biaxiality [11]. However, topologically integer lines are allowed in BN [9], thus the test relies on energetic rather than topological features, i.e., the appearance of defects should depend not only on the symmetry of the nematic phase, but also on the relative values of elastic constants and of surface anchoring. There is then a strong need for a detailed analysis of the differences to be expected in biaxial and uniaxial thin films, as used in experiments. Here we investigate the features in the defect structure of UN and BN by Monte Carlo (MC) [3,12] and analytical techniques [9]. We simulate the schlieren textures [11] of nematic films with tangential (in-plane) boundary conditions (BC) starting from the lattice model Hamiltonian,

$$U_N = \sum_{\substack{i,j \in \mathcal{F} \\ i \neq j}} \Phi_{ij} + J \sum_{\substack{i \in \mathcal{F} \\ j \in \mathcal{S}}} \Phi_{ij}, \qquad (1)$$

where $\mathcal{F}$, $\mathcal{S}$ are the set of particles (spins) in the bulk and at the surfaces, respectively, and Φ_{ij} is the pair potential [3] depending on the relative orientation ω_{ij} of the two particles,

$$\Phi_{ij} = -\epsilon_{ij}\{P_2(\cos \beta_{ij}) + 2\lambda[R_{02}^2(\omega_{ij}) + R_{20}^2(\omega_{ij})]$$
$$+ 4\lambda^2 R_{22}^2(\omega_{ij})\}. \qquad (2)$$

The particle positions are fixed at the sites of a simple $N \times N \times d$ cubic lattice and the strength of interaction ϵ_{ij} is $\epsilon \geq 0$, when i and j are the nearest neighbors and zero otherwise. $\omega \equiv (\alpha, \beta, \gamma)$ is the set of Euler angles for the orientation of a particle. P_2 is a second Legendre polynomial and R_{mn}^L are combinations of Wigner functions, symmetry adapted for the D_{2h} group of the two particles [3,12]. λ is a molecular biaxiality parameter, when $\lambda = 0$, Φ_{ij} reduces to the Lebwohl-Lasher potential for UN [13]. Tangential BC are set by fixing random (x, y) in-plane orientations of the director $\mathbf{n}$ (orientation of the longest molecular axes) at the top and bottom surfaces and a random alignment of the orthogonal directors $\hat{\mathbf{l}}$ and $\hat{\mathbf{m}}$. We leave empty space at the four lateral faces of the lattice which is updated following Metropolis [14,15]. We simulate lattices of various sizes for $\lambda = 0, 0.2, 0.25, 0.3$ at some selected temperatures $T^* = kT/\epsilon$ and different couplings with the surfaces, in particular, $J = 1/2$. Simulations start with bulk spins perpendicular to the surfaces to avoid any in-plane bias. The polarizing microscope textures were simulated using Müller matrices [12,16].

UN simulations show that a typical coarsening network involves mainly defects with four dark brushes and strength $k = \pm 1$ (the director rotates by 2π around the defect center), Fig. 1. The defects disappear by pair annihilation $+1-1 = 0$, as illustrated by the pair enclosed by a square in Fig. 1(b). The defects $k = \pm 1$ are not singular, as $\hat{\mathbf{n}}$ reorients along the vertical axis, Fig. 1(d). In contrast to the well known "escape into third dimension" in a cylindrical sample [17,18], surface anchoring at the bounding plates hinders reorientation by forming a pair of point defects—boojums—capping the line at the plates.

For BN simulations [3], Fig. 2 clearly shows a difference with UN: although $k = \pm 1$ defects do appear at the beginning of simulations, they quickly split into two-brushed defects with $k = \pm 1/2$. Similarly to the escape into third dimension in UN, $\hat{\mathbf{n}}$ in $k = \pm 1$ defects reorients along the axis, Fig. 3; however, this escape of $\hat{\mathbf{n}}$ implies a singularity in $\hat{\mathbf{l}}$ and $\hat{\mathbf{m}}$.
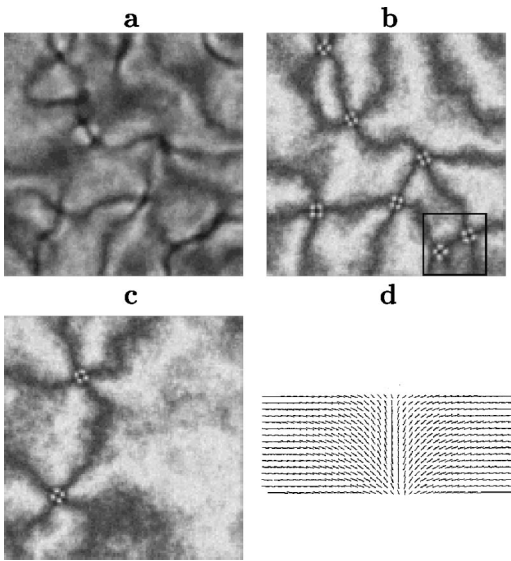
FIG. 1. Evolution of a UN texture for a $120\times120\times16$ lattice at $T^*=0.4$ and $J=1/2$ after 2 (a), 5 (b), and 60 (c) kcycles. Optical parameters: refractive indices $n_x=n_y=1.5$ and $n_z=1.7$ [16], film thickness $d=5.3\mu m$ and light wavelength 545 nm. (d) Vertical cross section of the $k=1$ defect.

Qualitatively, such a hybrid character (escaped $\hat{\mathbf{n}}$ and singular $\hat{\mathbf{l}}$, $\hat{\mathbf{m}}$) of $k=\pm1$ disclinations can be explained by the fact that the elastic constant K_n associated with $\hat{\mathbf{n}}$ is larger than K_l, K_m [19]. K_n is unlikely to be very different from the values K in UN, whereas K_l, K_m are generally smaller, especially near the BN-UN transition. The $k=\pm1/2$ lines do not show escape of $\hat{\mathbf{n}}$. Apparently, the splitting of $k=\pm1$ lines into $k=\pm1/2$ pairs reduces the elastic energy associated with K_n; this and other elastic features are analyzed below. We start with UN elasticity and to study the schlieren textures in a cell with an infinitely strong degenerate tangential anchoring, we consider a cylindrical domain of radius $R\gg d$ and radial ori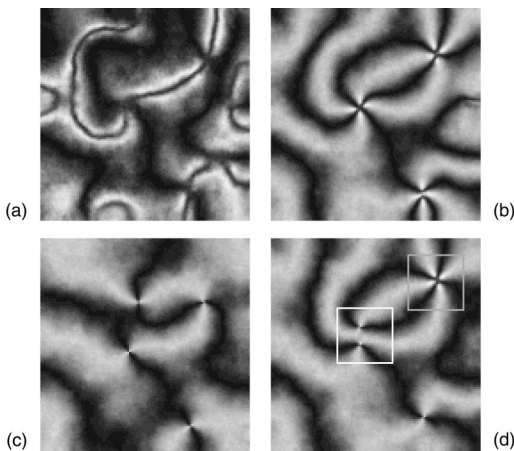entation of $\hat{\mathbf{n}}$ at R. The equilibrium structure should (a) minimize the elastic energy functional, written in the one-constant approximation and in cylindrical coordinates (r,ϕ,z) as

$$F^u=\frac{K}{2}\int_0^{2\pi}d\phi\int_{-d/2}^{d/2}dz\int_0^R[(\mathrm{div}\,\hat{\mathbf{n}})^2+(\mathrm{curl}\,\hat{\mathbf{n}})^2]rdr \quad (3)$$

and (b) satisfy the BC $n_r(r,\phi,\pm d/2)=n_r(R,\phi,z)=1$. There are two planar structures that satisfy BC at $z=\pm d/2$: a singular $k=1$ line with the energy [20]

$$F^u_{sing}=\pi Kd(\ln(R/r_1)+u_1), \quad (4)$$

and a pair of singular lines $k_1=k_2=1/2$ at a distance $L\ll R$ with [21]

$$F^u_{pair}=\pi Kd\left(\frac{1}{2}\ln\frac{2R^2}{r_{1/2}L}+2u_{1/2}\right), \quad (5)$$

$r_1\sim r_{1/2}$ are the molecular radii of the singular cores that carry the normalized core energy $u_1\sim u_{1/2}\sim1$.

An analytical solution for the escaped disclinations is known only for infinitely long cylindrical samples but not for flat films with anchoring at $z=\pm d/2$. To find the solution for the axially symmetric $k=1$ line in a flat sample, we employ the free energy

$$F_{ax}=\pi K\int_{-d/2}^{d/2}dz\int_0^R dr\left[r\theta_{,z}^2+r\theta_{,r}^2+\frac{\sin^2\theta}{r}\right.$$

$$\left.-2\theta_{,z}\sin^2\theta+\theta_{,r}\sin2\theta\right], \quad (6)$$

valid for any axially symmetrical solution, escaped or not, with $\theta(r,z)$ the angle between $\hat{\mathbf{n}}$ and the z axis. The subscripts after comma denote the corresponding spatial derivatives and the two last terms are complete differentials. For the escaped line in a film with an infinitely strong tangential
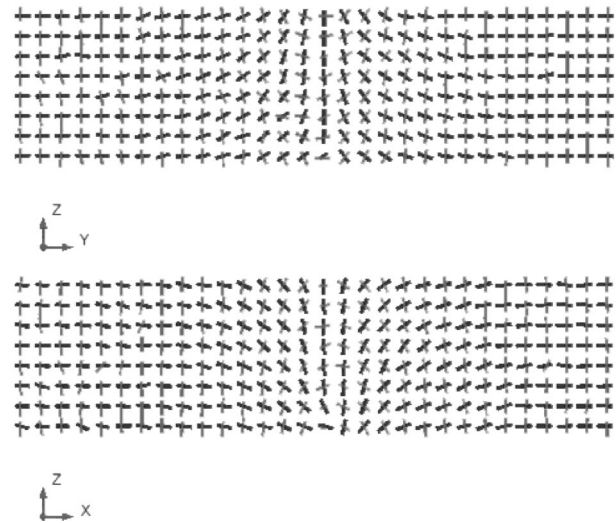

FIG. 3. Snapshots of the long (black) and short (grey) axis of two orthogonal vertical sections of the biaxial lattice model centered at the four brushes defect indicated in Fig. 2(c).

FIG. 2. [(a)-(d)] from top left to bottom right). Evolution of a BN texture ($\lambda=0.2$) for a $120\times120\times8$ lattice at $T^*=0.1$ and $J=1/2$ after 5 (a), 9 (b), 13 (c), and 60 (d) kcycles. Here we employ $n_x=1.54$, $n_y=1.51$, and $n_z=1.61$.

anchoring $[\theta(0,z)=0, \theta(r,\pm d/2)=\theta(R,z)=\pi/2]$, the $\theta_{,z}$ term integrates to zero and the $\theta_{,r}$ term contributes $\pi K d$. For $r \gg d$, the surface anchoring dominates, $\theta(r,z) \to (\pi/2)$, and the bulk equilibrium equation

$$r^2 \theta_{,zz} + r^2 \theta_{,rr} + r \theta_{,r} = \sin \theta \cos \theta \qquad (7)$$

has a linearized solution $\Psi(r,z) = \pi/2 - \theta(r,z)$, which is even in z because of the symmetric BC at $z=\pm d/2$,

$$\Psi(r,z) = \sum_{m \geq 0} A_m K_\nu(q_m r) \cos q_m z, \qquad (8)$$

where $\nu = i = \sqrt{-1}$, $q_m = \pi(2m+1)/d$, and A_m are numerical coefficients. The modified Bessel function $K_i(q_m r)$ and thus Ψ have an exponential asymptotic decay [22].

Dimensional analysis allows us to write the energy of escaped $k=1$ line as

$$F_{esc} = \pi K d [\ln(R/d) + g], \qquad (9)$$

where g is the universal numerical constant to be determined. To calculate g, we use the direct variational method. We construct the probe function following the idea of Kleman [9] that the escaped $k=1$ line perpendicular to a boundary is capped by a surface point defect—boojum. The function

$$\theta_1(r,z) = \arctan \frac{\eta d r}{(d/2)^2 - z^2}, \qquad (10)$$

with a dimensionless variational parameter η simulates an escaped disclination capped by a radial boojum at $z=-d/2$ and a hyperbolic boojum at $z=d/2$, but has to be modified to yield the exponential decay of $\Psi = (\pi/2) - \theta$ as $r \to \infty$. We do this in two different ways: (i) We restrict $\theta_1(r,z)$ to a cylindrical region $0 < r < a$ and use $\Psi(r,z)$ outside it, choosing the A_m to provide continuity at $r=a$. (ii) We directly insert the exponential saturation to $\pi/2$ into $\theta_1(r,z)$ to get

$$\theta_2(r,z) = \arctan \frac{\eta d r \exp(r/a)}{(d/2)^2 - z^2}. \qquad (11)$$

The minimum values of g and the corresponding values of variational parameters a and η are: (1) $g=4.187$, $a/d=0.1925$, $\eta=0.9894$ and (2) $g=4.196$, $a/d=0.7105$, $\eta=0.8181$. The values of g for the different probe functions are very close, and we conclude that $g=4.1$ within 2% accuracy. According to Eqs. (4), (5), and (9), the escaped structure is more stable than a singular $k=1$ line when $d > r_1 \exp(g-u_1)$ and than a pair of singular lines $k_1 = k_2 = 1/2$ when $d > \sqrt{r_{1/2} L/2} \exp(g - 2u_{1/2})$. Both conditions are satisfied even for submicron cells, $d > 200 - 500$ nm (cf. Fig. 1). Soft anchoring would facilitate the escape even for smaller d. Note that the analysis above is valid when the elastic constants are close, as in many low molecular weight materials.

We now turn to BN, whose elastic energy density can be approximated by neglecting the mixed elastic constants [23]; in a one-constant model for each director,

$$f^b \approx \tfrac{1}{2} \{ K_n [(\text{div } \hat{\mathbf{n}})^2 + (\text{curl } \hat{\mathbf{n}})^2] + K_m [(\text{div } \hat{\mathbf{m}})^2 + (\text{curl } \hat{\mathbf{m}})^2]$$

$$+ K_l [(\text{div } \hat{\mathbf{l}})^2 + (\text{curl } \hat{\mathbf{l}})^2] \}. \qquad (12)$$

We consider a strong homeotropic anchoring for $\hat{\mathbf{l}}$ $[l_z(r,\phi,\pm d/2)=1]$ and radial orientation of $\hat{\mathbf{n}}$ at the outer cylinder, $[n_r(R,\phi,z)=1]$. The energy of planar ($\hat{\mathbf{l}}=\hat{\mathbf{e}}_z$) disclinations in BN is obtained replacing K in Eqs. (4), (5) with $K_n + K_m$. The escaped configuration in BN lowers the energy by replacing the singularity in $\hat{\mathbf{n}}$ with that in the short director $\hat{\mathbf{l}}$ [19]. When $K_l \approx K_m$, $\hat{\mathbf{m}}$ in the escaped configuration remains normal to $\hat{\mathbf{e}}_z$ ($\hat{\mathbf{m}}=\hat{\mathbf{e}}_\phi$) and the free energy depends on the angle $\theta(r,z)$ between $\hat{\mathbf{n}}$ and z axis

$$F_{ax}^b = \pi (K_n + K_l) \int_{-d/2}^{d/2} dz \int_{r_h}^{R} dr \left[r(\theta_{,z}^2 + \theta_{,r}^2) + w \frac{\sin^2 \theta}{r} \right.$$

$$\left. - 2 \theta_{,z}(1 - w \cos^2 \theta) + w \theta_{,r} \sin 2\theta \right]$$

$$+ \pi d (K_l + K_m)[\ln(R/r_h) + u_h], \qquad (13)$$

where $w = (1-\xi)/(1+\xi)$ and $\xi = K_l/K_n$ determine the effect of biaxiality; $0 \leq \xi \leq 1$ is qualitatively similar to λ in MC simulations. The two last terms of the integrand are complete differentials. For the escaped configuration with BC $\theta(r_h,z)=0$, $\theta(r,\pm d/2)=\theta(R,z)=\pi/2$, the $\theta_{,z}$ term integrates to zero, and the $\theta_{,r}$ term contributes $\pi(K_n - K_l)d$. Similarly to UN, the free energy of the escaped configuration is

$$F_{esc}^b = \pi d [K_n \ln(R/d) + K_l \ln(d/r_b) + K_m \ln(R/r_b)$$

$$+ K_n g(\xi) + (K_l + K_m) u_b], \qquad (14)$$

where r_b and u_b are the radius and the normalized energy of the core singular in both $\hat{\mathbf{l}}$ and $\hat{\mathbf{m}}$; $g(\xi)$ is the universal dimensionless function determined below. To calculate $g(\xi)$, we use again the approaches (1) and (2) of the UN case, namely, the probe functions $\theta_1(r,z)$ supplemented by $\Psi(r,z)$ and $\theta_2(r,z)$. The only difference is that in the linearized solution for $\Psi(r,z)$, Eq. (8) K_ν should have $\nu = i\sqrt{w}$, because the bulk equilibrium Eq. (7) in BN is of the form $r^2 \theta_{,zz} + r^2 \theta_{,rr} + r \theta_{,r} = w \sin \theta \cos \theta$. Minimization of F_{esc}^b with respect to a and η leads to the $g(\xi)$, $a(\xi)$, and $\eta(\xi)$ shown in Fig. 4. When $\xi \to 1$, then the nonlinear term w decreases, $w \to 0$. Therefore, the linearized solution $\Psi(r,z)$ (8) is close to the exact one even for small r/d. As seen in Fig. 4, function no. 1 produces smaller values of g than no. 2 and the optimum radius of inner cylinder a for the probe function no. 1 shrinks as ξ increases. We now analyze the stability of BN defects, Eqs. (4), (5), and (14) assuming $r_1 \approx r_{1/2} \approx r_b$, $u_1 \approx u_{1/2} \approx u_b$, and remembering that $K \to K_n + K_m$. We find the following cases.

(a) The escaped configuration is more stable than a singular $k=1$ line when $d > d_{c1} = r_b \exp\{[g(\xi)/(1-\xi)] - u_b\}$. The condition $d > d_{cr}$ is satisfied in samples of reasonable size (microns), if the biaxiality is not very strong. For example,
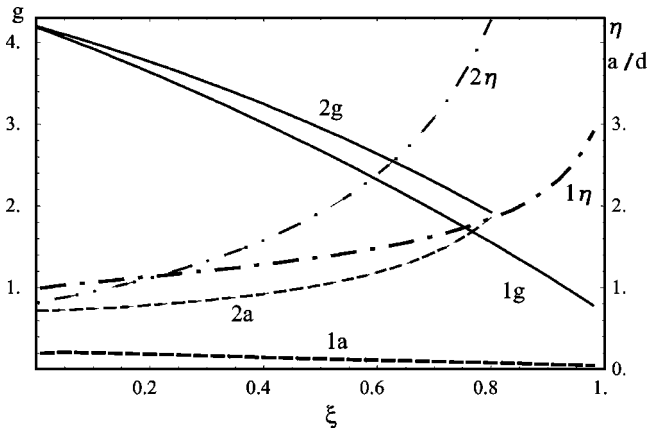
FIG. 4. Dependencies $g(\xi)$, $a(\xi)$, and $\eta(\xi)$ for probe functions no. 1 and no. 2 (see text).

even if $\xi = 0.8$ and $g \approx 1.5$, see Fig. 4, the critical thickness is rather small: $d_{c1} \sim 10^3 r_b$. This result agrees with the MC data that $\hat{\mathbf{n}}$ escapes in the disclinations $k = \pm 1$. For strong biaxiality, $\xi \rightarrow 1$, d_{c1} diverges: K_l and K_m become close to K_n and the escape brings no energy gains.

(b) As compared to singular lines $k_1 = k_2 = 1/2$ separated by L, the escaped configuration is stable when $d > d_{c2} = \sqrt{r_b L/2}\,(L/r_b)^{\xi/(1-\xi)} \exp[(g-2u_b)/(1-\xi)]$. If $\xi \lesssim 0.1$ (say, near the BN-UN transition), the escaped lines might be preferred in samples of reasonable size. When the biaxiality is strong, any macroscopic L makes the pair $k_1 = k_2 = 1/2$ preferable to the escaped line. E.g., with $\xi = 0.3$, one estimates $d_{c2} \sim 5L$, a large quantity indeed. However, even in the strongly biaxial system, the escaped configuration might still

be involved in the transformation of the planar $k = \pm 1$ line into the pair $k_1 = k_2 = 1/2$. Escape of $k = \pm 1$ line is a process with no energy barrier, while the splitting of a planar $k = \pm 1$ line into a pair of cores has a barrier $\sim K$ per unit length. MC simulations, Figs. 2 and 3, demonstrate indeed that the $k = \pm 1$ lines first escape into the third dimension and then split into pairs of $k_1 = k_2 = \pm 1/2$ disclinations.

In summary, for UN schlieren textures, we have found an explanation for the observation that defects with four brushes correspond to surface point defects with escaped director in the bulk. Even an infinitely strong surface anchoring cannot prevent such an escape in the slabs of reasonable (submicron and more) thickness. In BN, the $k = \pm 1$ disclinations can be hybrid: $\hat{\mathbf{n}}$ director escapes, whereas the "short" directors form a singularity along the defect axis. Such an escape is favorable when the biaxiality is weak, i.e., the elastic constants for "short" directors are noticeably smaller than that for $\hat{\mathbf{n}}$. If the biaxiality is strong, the planar disclinations can split into pairs of $k = \pm 1/2$ lines. However, the splitting is not a universal feature of the biaxial phase: first, the escaped configurations might be stable for weak biaxiality; second, they might appear as transient features when a $k = \pm 1$ line splits into a pair of singular $k = \pm 1/2$ lines. Computer simulations have allowed us to run virtual experiments showing differences in the optical textures of BN and UN and testing the theory.

[1] See, e.g., Mol. Cryst. Liq. Cryst. Sci. Technol., Sect. A **323**, 153 (1998).
[2] M.J. Freiser, Phys. Rev. Lett. **24**, 1041 (1970).
[3] F. Biscarini *et al.*, Phys. Rev. Lett. **75**, 1803 (1995).
[4] M.P. Allen, Mol. Phys. **52**, 717 (1984); Liq. Cryst. **8**, 499 (1990).
[5] R. Berardi and C. Zannoni, J. Chem. Phys. **113**, 5971 (2000).
[6] Y. Galerne, Mol. Cryst. Liq. Cryst. Sci. Technol., Sect. A **323**, 211 (1998).
[7] S.M. Fan *et al.*, Chem. Phys. Lett. **204**, 517 (1993).
[8] J.R. Hughes *et al.*, J. Chem. Phys. **107**, 9252 (1997).
[9] M. Kleman, *Points, Lines and Walls, In Liquid Crystals, Magnetic Systems, and Various Ordered Media* (Wiley, New York, 1982).
[10] *Defects in Liquid Crystals: Computer Simulations, Theory and Experiments*, edited by O.D. Lavrentovich, P. Pasini, C. Zan-
noni, and S. Žumer (Kluwer, Dordrecht, 2001).
[11] S. Chandrasekhar *et al.*, Curr. Sci. **75**, 1042 (1998).
[12] C. Chiccoli *et al.*, Phys. Rev. Lett. **79**, 4401 (1997).
[13] P.A. Lebwohl and G. Lasher, Phys. Rev. A **6**, 426 (1972).
[14] N. Metropolis *et al.*, J. Chem. Phys. **21**, 1087 (1953).
[15] *Advances in the Computer Simulations of Liquid Crystals*, edited by P. Pasini and C. Zannoni (Kluwer, Dordrecht, 2000).
[16] E. Berggren *et al.*, Phys. Rev. E **50**, 2929 (1994).
[17] R.B. Meyer, Philos. Mag. **27**, 405 (1973).
[18] P.E. Cladis and M. Kléman, J. Phys. (Paris) **33**, 591 (1972).
[19] S. Sukumaran and G.S. Ranganath, J. Phys. II **7**, 583 (1997).
[20] F.C. Frank, Discuss. Faraday Soc. **29**, 945 (1958).
[21] C.F. Dafermos, Q. J. Mech. Appl. Math. **23**, 549 (1970).
[22] M. Abramowitz and I.A. Stegun, *Handbook of Mathematical Functions* (Dover, New York, 1970).
[23] L. Longa *et al.*, J. Chem. Phys. **109**, 1555 (1998).